



Recursive Bayesian electromagnetic refractivity estimation from radar sea clutter

Sathyanarayanan Vasudevan,¹ Richard H. Anderson,² Shawn Kraut,³ Peter Gerstoft,⁴ L. Ted Rogers,⁵ and Jeffrey L. Krolik⁶

Received 21 November 2005; revised 3 May 2006; accepted 29 November 2006; published 27 April 2007.

[1] Estimation of the range- and height-dependent index of refraction over the sea surface facilitates prediction of ducted microwave propagation loss. In this paper, refractivity estimation from radar clutter returns is performed using a Markov state space model for microwave propagation. Specifically, the parabolic approximation for numerical solution of the wave equation is used to formulate the refractivity from clutter (RFC) problem within a nonlinear recursive Bayesian state estimation framework. RFC under this nonlinear state space formulation is more efficient than global fitting of refractivity parameters when the total number of range-varying parameters exceeds the number of basis functions required to represent the height-dependent field at a given range. Moreover, the range-recursive nature of the estimator can be easily adapted to situations where the refractivity modeling changes at discrete ranges, such as at a shoreline. A fast range-recursive solution for obtaining range-varying refractivity is achieved by using sequential importance sampling extensions to state estimation techniques, namely, the forward and Viterbi algorithms. Simulation and real data results from radar clutter collected off Wallops Island, Virginia, are presented which demonstrate the ability of this method to produce propagation loss estimates that compare favorably with ground truth refractivity measurements.

Citation: Vasudevan, S., R. H. Anderson, S. Kraut, P. Gerstoft, L. T. Rogers, and J. L. Krolik (2007), Recursive Bayesian electromagnetic refractivity estimation from radar sea clutter, *Radio Sci.*, 42, RS2014, doi:10.1029/2005RS003423.

1. Introduction

[2] The determination of microwave propagation conditions in the troposphere is important for assessing the performance of both communications and radar systems. In general, radar coverage over the sea surface is determined by the atmospheric refractive index, n , which although very close to unity, depends on meteorological conditions. Although in a well-mixed atmosphere,

microwave propagation is typically limited to the line of sight, in coastal regions where hot, dry air is advected from the land over cool, humid air near the sea surface, it is not uncommon for the refractive index to decrease very quickly with height. Under such conditions, ducted propagation can occur, resulting in propagation beyond the horizon. Figure 1 illustrates the effect of ducting on radar backscatter returns from the sea surface off the Virginia coast. Figure 1 is a plot of power versus range and azimuth from a 3 GHz radar pointed at the horizon. The significant clutter returns from ranges well beyond the approximately 48 km (30 mile) horizon are the result of surface-based ducting conditions. Prediction of propagation loss to points above the sea surface over the coverage area shown in Figure 1 can be achieved using an estimate of the profile of index of refraction as a function of height, range, and azimuth in a computational electromagnetic propagation model.

[3] Conventional methods for estimating modified refractivity, M , defined by $M = 10^6 \times (n - 1)$, where n is the refractive index, can be split into two categories: (1) direct sensing techniques which involve the measure-

¹Sensor Research and Development Corporation, Orono, Maine, USA.

²Applied Signal Technology, Inc., Arlington, Virginia, USA.

³Lincoln Laboratory, Massachusetts Institute of Technology, Lexington, Massachusetts, USA.

⁴Marine Physical Laboratory, Scripps Institution of Oceanography, University of California, San Diego, La Jolla, California, USA.

⁵Space and Naval Warfare Systems Center, San Diego, California, USA.

⁶Department of Electrical and Computer Engineering, Duke University, Durham, North Carolina, USA.

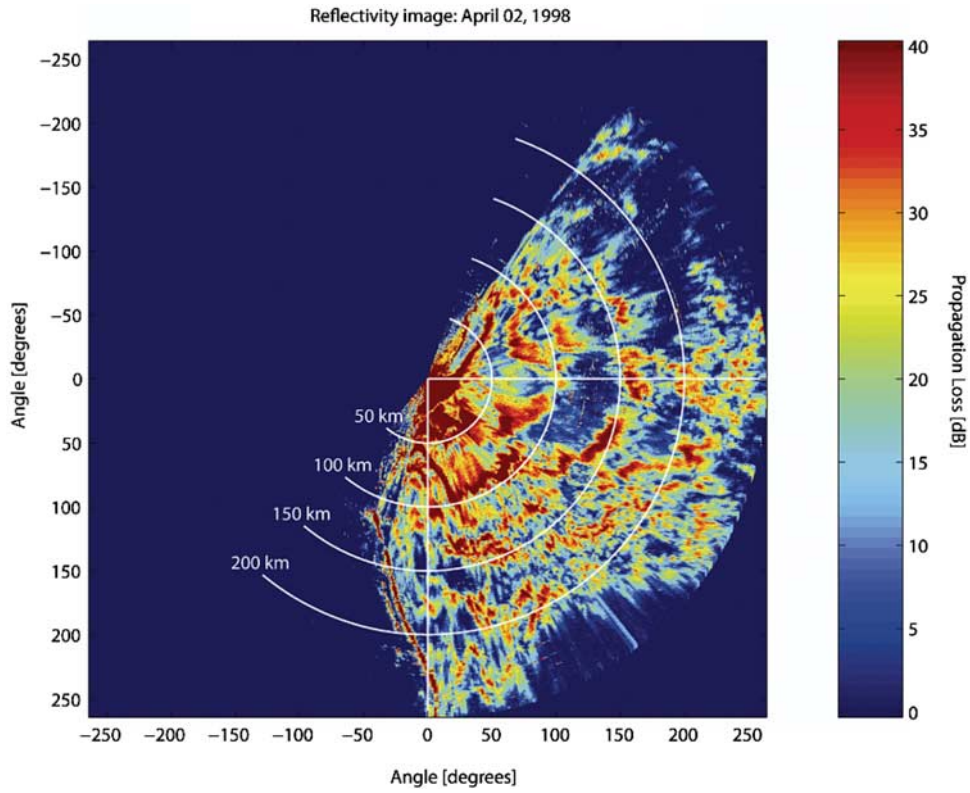


Figure 1. Plan position indicator data from SPANDAR radar on Wallops Island, Virginia, at 2110 UT on 2 April 1998.

ment of atmospheric pressure, temperature and humidity to determine the index of refraction; and (2) remote sensing techniques which infer refractivity more indirectly. Instruments for making direct measurements include radiosondes [Rowland and Babin, 1987], microwave refractometers, and rocketsondes. A drawback of these devices, however, is that they are often expensive and/or difficult to deploy [Halvey, 1983]. Moreover, these measurements tend to provide estimates of refractivity versus height at a single range while propagation depends on range-varying profiles at each azimuth. Among remote sensing methods, Doppler spread radar returns have historically provided very detailed pictures of the dynamics and structure of the turbulent boundary layer which, in principle, can be used to infer refractivity. In practice, however, the Doppler spread returns are often contaminated by nonturbulence-related components [Skolnik, 1980]. Alternatively, lidar can provide a means of estimating profiles of atmospheric water vapor that can then be used to infer refractivity. However the performance of lidar is severely restricted by background noise levels and high extinction (e.g., cloud) conditions. Ground-based point-to-point microwave propagation measurements using multiple transmitter/receiver pairs

[Tabrikian and Krolik, 1999], as well as the usage of ground-based measurements of GPS signals as the satellites rises and sets on the horizon in inferring refractivity [Anderson, 1994] has successfully overcome the single time and space line representation of refractivity. The inferred profiles would be characteristic of the integrated refractive effects along the vertical and horizontal paths. In this regard, inferring refractivity from radar clutter provides an extension of these strategies where now the radar itself is used as a remote sensing device.

[4] The desirability of not having to use additional equipment to estimate refractivity motivates the estimation of range and height varying refractivity from clutter (RFC). Previous work concerning the phenomenology of sea clutter returns from extended ranges associated with ducting conditions has been discussed in the work of Gossard and Strauch [1983]. In addition, it has been shown that temporal and spatial variations of radar echoes are related to temporal and spatial variations in the layers of the refractivity profile [Richter, 1969]. The advantage of RFC, as discussed in this paper, is that it provides a synoptic characterization of the duct over the spatial extent of the radar and it overcomes the necessity

of additional data and/or sensing devices. In addition, RFC has the added advantage of being able to sense range-varying refractivity at a temporal sampling rate that can track changes in atmospheric conditions.

[5] In previous work, RFC estimation was made by using a maximum a posteriori (MAP) approach to jointly estimate the refractivity and the spatially varying backscatter cross section [Tabrikian *et al.*, 1999]. The main drawback of the method proposed in that paper was that only linear variations in refractivity parameters could be obtained. When the algorithm was modified to track more complicated range-varying refractivity, the estimation was found to be computationally intractable. Subsequent methods to improve estimation of more complicated range-varying behavior of refractivity was undertaken by formulating the RFC problem as a nonlinear state space problem whose solution was obtained using sequential importance sampling technique for state space estimation [Vasudevan and Krolík, 2001]. The approach provided a quick and efficient method of estimating complicated range-varying refractivity. However, the method failed to update previous estimates of refractivity with the arrival of new data and hence the accuracy of the estimates decreased rapidly with increasing range. More recently, a genetic algorithm (GA) approach to estimate refractivity RFC has been proposed [Gerstoft *et al.*, 2003a, 2003b]. In that work, the authors have presented a method to model the range and height varying refractivity of the environment using a total of 11 parameters [Gerstoft *et al.*, 2003b] while imposing some prior constraints [Gerstoft *et al.*, 2003a] in order to increase the accuracy of results over the coverage area of the radar. The parameters are estimated by performing a global search using a nonlinear GA optimization approach. In contrast to the need for global optimization, in this paper the range-recursive nature of the parabolic equation is exploited to yield a potentially more computationally efficient solution. More recently [Barrios, 2004], a method has been proposed which utilizes the rank correlation between the clutter power observed and the density of raypaths to estimate refractivity. The approach discussed in that paper is designed primarily for surface-based ducts because of its utilization of land clutter to estimate refractivity over a coverage area which includes a land-sea boundary. The method presented in this paper has the added advantage that, in principle it can be used over both sea and land-sea transition by virtue of the Markovian modeling of the range-varying refractivity profile.

[6] The remainder of this paper is organized as follows. In section 2, a simple parameterization of the index of refraction is described which covers a variety of different ducting conditions. This is followed by presentation of a nonlinear recursive state space model for the electromagnetic field which is derived from the split-step

Fourier algorithm used to solve the wave equation in inhomogeneous media. Section 3 describes the Monte Carlo recursive Bayesian particle filtering approach used to estimate range-varying refractivity from sea clutter returns. Finally, section 4 is a discussion of simulation results and the demonstration of the method using real radar data collected off the Virginia coast.

2. Statistical State Space Modeling of Tropospheric Propagation

2.1. Tropospheric Refractivity Model

[7] Although the marine atmospheric boundary layer (MABL) variability which causes microwave ducting is often complex in nature, for the purposes of propagation studies, it is often represented at a given range by bilinear and/or trilinear height-dependent refractivity profiles [Rogers, 1996]. In the absence of ducting, standard propagation conditions are represented by a linear profile which appears upward refracting in Earth-flattened coordinates [Anderson, 1994; Rogers, 1996]. In the presence of a surface-based duct, the sudden change in refractivity which defines the duct is most commonly modeled by the MABL structure shown in Figure 2. This simple trilinear parameterization is quite versatile in its ability to include refractivity representations of the standard Earth atmosphere, surface-based ducts, elevated ducts and evaporation ducts. Surface-based ducts are ducts which are formed at heights within a few hundred meters of the surface of the Earth while ducts whose heights reach up to 5000 feet are termed as elevated ducts. Evaporation ducts are similar to surface-based ducts, but their heights are restricted to values ranging up to 40 m. Evaporation ducting is not readily discernable from a radar's plan position indicator (PPI), but still results in frequency-dependent extensions of radar range.

[8] Instead of determining the refractivity at each point over height at a given range, it has been shown [Rogers, 1996] that the parameterization of the profile can be limited to a few variables without adversely affecting performance. The refractivity structure for the MABL shown in Figure 2 is parameterized into 3 basic parameters, namely, the base height, thickness and the M deficit. The base height is defined as the height from the surface of the sea to the lower boundary of the trapping layer. The thickness is defined as the distance between the lower and the upper boundaries of the trapping layer. M deficit is the difference in the modified refractivity values at the two boundaries of the trapping layer. The base height and the M deficit to a large degree account for the magnitude of the ducted field. The base height, thickness and M deficit determine the height of the duct in the troposphere and the number of rays that would be trapped in the duct. In addition, they also affect

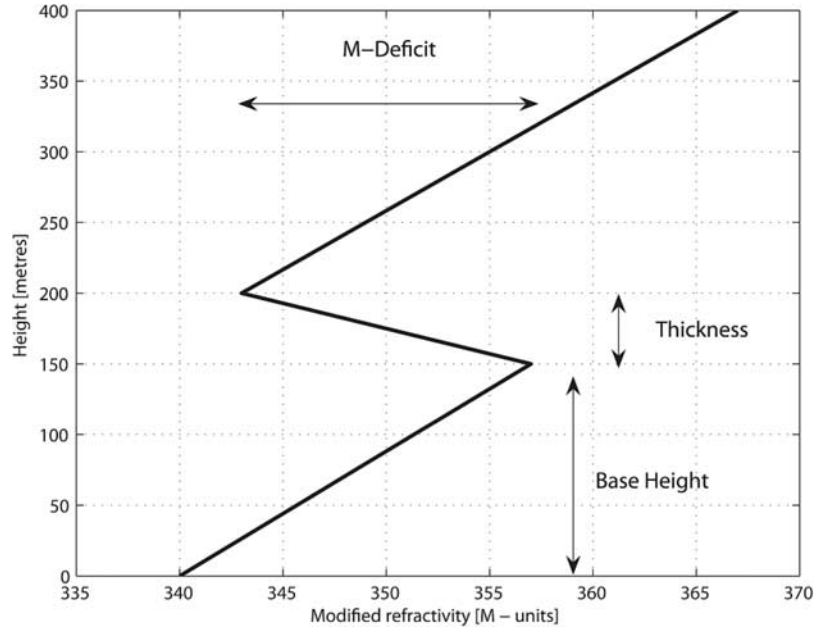


Figure 2. Refractivity modeling of the marine atmospheric boundary layer (MABL).

the curvature of rays in the trapping layer. A fourth parameter is the slope of refractivity in the lowest layer. The above trilinear model is versatile in its ability to model typical ducting conditions that have been observed. For example, when the base height reduces to zero, we end up with a bilinear surface-based duct, which models the scenario where the internal boundary layer (IBL) controls propagation. When the base height rises to values above 1000 ft, the trilinear structure models the behavior of an elevated duct. In practice, the refractivity profile often changes with range. In this paper, a range-varying extension of bilinear/trilinear profile is achieved here by modeling the parameters as a Markov process. This modeling, while being physically plausible, has the added advantage of facilitating computationally efficient estimation of range-varying refractivity. In the above modeling, it is assumed that the value of the modified refractivity at the sea level is known to be at 340 M units. The reason for this assumption is that the authors have found that the most important information is in the slopes of the refractivity rather than their absolute values. As a result, any commonly observed value in the range of 280–360 can be used. In addition, the value of the refractivity in the third layer is assumed to be constant value of 0.113 M units/m. This is a valid assumption since most electromagnetic fields that enter this region makes no contribution to the field being measured at the surface. Hence, for purposes of modeling, any realistic observed value that does not make any significant con-

tributions of electromagnetic signals at the surface can be used.

2.2. Nonlinear State Space Formulation of Field Propagation

2.2.1. State Equation Formulation

[9] The most commonly used approach to model wave propagation in the troposphere is the Fourier split-step solution to the parabolic equation [Dockery and Kuttler, 1996; Dockery, 1998]. This numerical solution is a forward solver with the ability to handle vertical and horizontal inhomogeneities in the refractive profile and is capable of delivering accurate propagation loss estimates in complicated environments.

[10] Let $u(r_k, z)$ be the electric field at range r_k and height z . Then, the field at range r_{k+1} and height z , denoted by $u(r_{k+1}, z)$, is given by the Fourier split-step solution to the parabolic wave equation,

$$u(r_{k+1}, z) = \exp\left[j\frac{k_o}{2}\left(\eta^2 + \frac{2z}{a_e} - 1\right)\delta r\right] \times \mathbf{F}^{-1}\left\{\exp\left[-j\frac{p^2\delta x}{2k_o}\right]\mathbf{F}\{u(r_k, z)\}\right\}, \quad (1)$$

where F is the spatial Fourier transform along the height z , $\delta r = r_{k+1} - r_k$ is the range increment, a_e is the radius of the Earth, η is the refractive index as a function of height and range, k_o is the wave number and p is the spatial frequency, or transform variable. It should be noted that

the split-step Fourier solution to the parabolic equation can be interpreted as multiplying the Fourier transform of the field at r_k by an exponential term that amounts to Fresnel diffraction of the wave in free space between the two ranges r_k and r_{k+1} . The inverse Fourier transform of this product, i.e., the field propagated in free space to r_{k+1} , is then multiplied by the phase changes brought about by aberration due to the inhomogeneous refractive medium. It should be noted that the phase aberration term contains the index of refraction profile between the two ranges. Thus, given the field at a range k , the field at range r_{k+1} is nonlinearly related to the index of refraction of the medium between the two ranges.

[11] As described previously, without loss of generality, let us assume that the index of refraction at range r_k is parameterized into $L = 4$ parameters, namely, the base height b_k , thickness t_k , M deficit dM_k and slope of refractivity in lower layer \dot{M}_k . The values taken by these parameters are assumed to be a piecewise range-independent approximation to the profile between the ranges r_k and r_{k+1} . Let $\mathbf{g}_k = [b_k, t_k, dM_k, \dot{M}_k]^T$ be the vector of these refractivity parameters at range r_k . Since the index of refraction is a function of physical quantities such as pressure, temperature and humidity, it is assumed here that the parameters of the refractivity do not undergo drastic changes over small range intervals. Moreover, the correlation of the refractive process suggests characterizing the relationship between the parameters from one range step to another by a Markov process. Then, the relationship between the refractivity parameters over range can be expressed as

$$\mathbf{g}_k = \mathbf{g}_{k-1} + \mathbf{w}_k, \quad (2)$$

where \mathbf{w}_k models the uncertainty in the variations of refractivity parameters over range. For simplicity, it is assumed to be a zero-mean Gaussian process with covariance matrix \sum_g .

[12] Let $\mathbf{u}_k = [u(r_k, z_1), u(r_k, z_2), \dots, u(r_k, z_M)]$ be the vector of complex field values at heights z_1, z_2, \dots, z_M at range r_k . The field as given in (1) is a function of all the refractivity parameters up to range r_{k-1} . Thus (1) can be written as

$$\mathbf{u}_k = f(\mathbf{g}_1, \mathbf{g}_2, \dots, \mathbf{g}_{k-1}, \mathbf{u}_0), \quad (3)$$

where the function $f(\cdot)$ represents the repeated application of the split-step solution to parabolic equation given in (1) out to range r_k and \mathbf{u}_0 is the field distribution at the starting range r_0 . In equation (3), the vector of refractivity parameter \mathbf{g}_k has L unknown parameters at each range r_k . Thus as the range increases, the number of unknowns increases by L times the number of range increments. Thus, for example, for $L = 4$, if the refractivity parameters change every kilometer, then with this approximation, by the time we reach 20 km,

which is the distance to the horizon for shipboard radar systems, the total number of parameters to be estimated is 80. Normally, estimates are required out to 150–200 km. As a result, the number of parameters to be jointly estimated is around 600–800. This is clearly a prohibitive number of parameters to estimate given the limited extent of the radar clutter data and computational resources.

[13] In order to expedite the solution for the $\mathbf{g}_1, \mathbf{g}_2, \dots, \mathbf{g}_k$, note that in the split-step solution to the wave equation, the field at range r_k can also be modeled as a Markov process if the complex field at the previous range step r_{k-1} is included as part of the state vector. In particular, using equation (1), equation (3) can be written as

$$\mathbf{u}_k = H(\mathbf{u}_{k-1}, \mathbf{g}_{k-1}), \quad (4)$$

where $H(\cdot)$ corresponds to the split-step operation as represented by equation (1). Combining equations (1), (2), and (4), we get the new state equation

$$\begin{bmatrix} \mathbf{g}_k \\ \mathbf{u}_k \end{bmatrix} = \begin{bmatrix} \mathbf{g}_{k-1} \\ H(\mathbf{u}_{k-1}, \mathbf{g}_{k-1}) \end{bmatrix} + \begin{bmatrix} \mathbf{w}_k \\ \mathbf{0} \end{bmatrix}. \quad (5)$$

[14] In the above formulation, it can be seen that the source and refractivity profile up to range r_{k-1} are incorporated into the field at r_k . A significant reduction in the dimensionality of the field vector \mathbf{u}_k at each range step r_k is possible when one utilizes the fact that because typical M deficits are on an average below 60 M units, only rays that have a grazing angle less than 1 degree typically propagate within the duct. In light of the above, instead of using the complex field vector over height z at each range, the complex vertical frequency wave number coefficients $\mathbf{v}_k = F\{\mathbf{u}_k\}$ are used instead, where F is the spatial discrete Fourier transform. An upper bound on the number of significant vertical wave number coefficients is given by the spatial frequency aperture-bandwidth product. This is analogous to the time-bandwidth product dimensionality of an approximately time and bandwidth limited process. The maximum vertical wave number is

$$k_{\nu_{\max}} = k \sin(\theta_{\max}), \quad (6)$$

where θ_{\max} is the maximum angle that actually propagates in the medium. The vertical spatial aperture in this case is the maximum expected duct height z_{\max} . Given this maximum vertical wave number, the discrete Fourier transform size used in the PE solver of equation (1) is determined using the spatial frequency-aperture product given by

$$z_{\max} k_{\nu_{\max}} = N_f \pi, \quad (7)$$

where z_{\max} is the maximum height to which propagation loss prediction is required and N_f is the Fourier transform size. For the current problem, the maximum angle that propagates in the duct is typically less than 1 degree and assuming the height to which propagation loss predictions are required is 200 m, the transform size is 64. Letting K denote the total number of clutter range bins, the advantage of using a Markov model with vertical wave number coefficients in the state vector is therefore that KL refractivity parameters can be solved recursively by updating a state vector of size $\dim(k_{\nu_{\max}} z_{\max}) + L \ll KL$ at each range versus a joint nonlinear optimization over all KL parameters. This yields a significantly more computationally efficient approach.

[15] Letting \mathbf{v}_k denote the vector of vertical wave numbers coefficients over height at range r_k , then in the spatial frequency domain, equation (4) can be written as

$$\begin{aligned} \mathbf{v}_k &= \mathbf{F}(H(\mathbf{F}^{-1}(\mathbf{v}_{k-1}), \mathbf{g}_{k-1})) \\ &= T(\mathbf{v}_{k-1}, \mathbf{g}_{k-1}), \end{aligned} \quad (8)$$

where F is the discrete spatial Fourier transform, $H(\cdot)$ corresponds to the split-step operation as represented by equation (1) and $T(\mathbf{v}_{k-1}, \mathbf{g}_{k-1}) \triangleq \mathbf{F}(H(\mathbf{F}^{-1}(\mathbf{v}_{k-1}), \mathbf{g}_{k-1}))$. Combining (2) and (8) into one equation, we have

$$\begin{aligned} \mathbf{g}_k &= \mathbf{g}_{k-1} + \mathbf{w}_k \\ \mathbf{v}_k &= T(\mathbf{v}_{k-1}, \mathbf{g}_{k-1}). \end{aligned} \quad (9)$$

[16] It should be noted that no state noise is applied to the second equation in (9) since this equation corresponds to the deterministic split-step PE computation. Finally, defining $\mathbf{x}_k \triangleq [\mathbf{g}_k, \mathbf{v}_k]$ as the state vector at range r_k , the state equations in (9) can be written compactly as

$$\mathbf{x}_k = h(\mathbf{x}_{k-1}) + \boldsymbol{\mu}_k \quad (10)$$

where $h(\cdot)$ is the nonlinear relationship between the state at range r_k and r_{k-1} and $\boldsymbol{\mu}_k = [\mathbf{w}_k, \mathbf{0}]^T$ is the state noise which is zero-mean Gaussian with covariance matrix $\Sigma = \begin{bmatrix} \Sigma_{\mathbf{g}} & \mathbf{0} \\ \mathbf{0} & \mathbf{0} \end{bmatrix}$.

2.2.2. Measurement Equation Formulation

[17] Having incorporated the propagation model in the state equation of (10), the measurement equation can be used to model the clutter return. A general expression for the radar clutter return, $y(r_k)$, at slant range bin r_k is given by

$$y(r_k) = \int_{r'} \int_{w'} H(r_k; r', w') b(r', w') dr' dw' + \nu(r_k), \quad (11)$$

where $b(r', w')$ is the complex coefficient of the sea surface, and the impulse response of the radar, $H(r_k; r', w')$, defines the output at r_k due to a point source at ground range and bearing (r', w') on the ocean surface. Note that $H(r_k; r', w')$ is a function of both radar parameters such as the beam former weights and pulse shape, as well as propagation model parameters such as refractivity. Because of surface roughness, $b(r', w')$ may be modeled as a complex zero-mean random process. Additive noise at the receiver is denoted by $\nu(r_k)$ and is modeled as complex zero-mean Gaussian distributed and uncorrelated with the clutter $b(r, w)$. The impulse response $H(r_k; r', w')$ can be modeled approximately as $H(r_k; r, w') \approx L(r_k; \mathbf{g}_1, \mathbf{g}_2, \dots, \mathbf{g}_k) h(r; r', w')$, where $L(r_k; \mathbf{g}_1, \mathbf{g}_2, \dots, \mathbf{g}_k)$ is the two-way propagation loss which depends on unknown refractivity profile vector parameters, $\mathbf{g}_1, \mathbf{g}_2, \dots, \mathbf{g}_k$, and $h(r; r', w')$ is the impulse response determined assuming propagation through free space and using the radar's beam and pulse width. Thus, for a series of n pulses, the radar return from equation (11), sampled at range bins (r_1, r_2, \dots, r_K) , is given by

$$y_n(r_k) = a_n(r_k) L(r_k; \mathbf{g}_1, \mathbf{g}_2, \dots, \mathbf{g}_k) + \nu_n(r_k), \quad (12)$$

where $n = 1, 2, \dots, N$ is the number of pulses transmitted by the radar. The clutter return at the n th snapshot (corresponding to the n th pulse transmitted)

$a_n(r_k) = \int_{\Omega} h(r_k; r', w') b(r', w') dr' dw'$ is modeled as a complex Gaussian random variable with a variance σ_a^2 which is assumed to be a constant over range. The variance of this clutter coefficient is the backscatter cross section of the sea surface and depends on the sea state, grazing angle, and the frequency at which the radar operates. Again, $L(r_k; \mathbf{g}_1, \mathbf{g}_2, \dots, \mathbf{g}_k)$ is the two-way propagation loss, which is a function of the unknown refractivity parameter vectors $\mathbf{g}_1, \mathbf{g}_2, \dots, \mathbf{g}_k$ which we are trying to estimate.

[18] Although (12) describes the complex clutter return, a more common output of radar systems is the plan position indicator (PPI) output, defined as the clutter power averaged in decibels (dB) over the number of radar pulses. The PPI is thus defined by

$$z_k = \frac{10}{N} \sum_{n=1}^N \log_{10} |y_n(r_k)|^2. \quad (13)$$

[19] It can be shown (see Appendix A) that under the model of (12), z_k in (13) is well approximated by a Gaussian distribution with mean $z_k = \frac{10}{\log(10)} \log(|L(r_k; \mathbf{g}_1,$

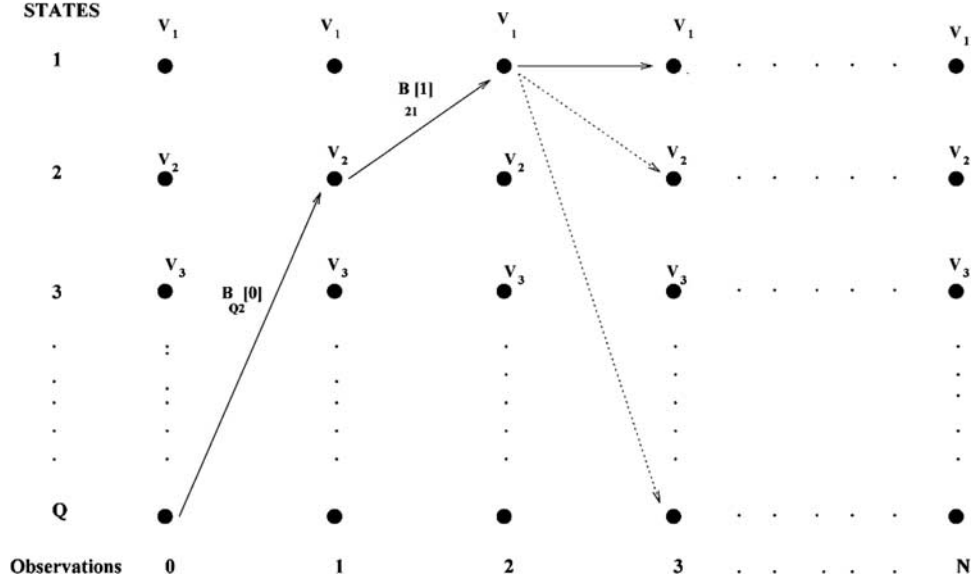


Figure 3. Discrete state space.

$\mathbf{g}_2, \dots, \mathbf{g}_k)^2 \sigma_a^2 + \sigma_v^2) - \frac{10\gamma}{\log(10)}$ and variance $\left(\frac{10}{N \log(10)}\right)^2 \left[\frac{\pi^2}{6} + (\log(2) - \gamma)^2\right]$, where γ is Euler's number. Given $L(r_k; \mathbf{g}_1, \mathbf{g}_2, \dots, \mathbf{g}_k)$, the returns from different nonoverlapping range bins are uncorrelated since they illuminate different surface scatterers. The mean of this process is thus a range varying function of propagation loss and depends on the vector of refractivity parameters $\mathbf{g}_1, \mathbf{g}_2, \dots, \mathbf{g}_k$ in a nonlinear manner. In terms of an observation equation, the PPI output at range r_k , can be written up to an additive constant in terms of the state vector \mathbf{x}_k from (10) as

$$\begin{aligned} z_k &= \frac{10}{\log(10)} \log \left[|\mathbf{C}^H \mathbf{G}(\mathbf{x}_k) \mathbf{G}^H(\mathbf{x}_k) \mathbf{C}|^2 \sigma_a^2 + \sigma_v^2 \right] + \varepsilon_k \\ &= \beta(\mathbf{x}_k) + \varepsilon_k, \end{aligned} \quad (14)$$

where $G(\mathbf{x}_k) = \mathbf{F}^{-1}(\mathbf{v}_k)$ is the inverse discrete Fourier transform of the wave number coefficients in the state which recreates the field distribution at range r_k over height, $\mathbf{C} = [0, 1, 0, 0, \dots, 0]^T$ is the vector used to select the intensity of the field near the sea surface from the state vector \mathbf{x}_k and where $\beta(\mathbf{x}_k) \triangleq \frac{10}{\log(10)} \log (|\mathbf{C}^H \mathbf{G}(\mathbf{x}_k) \mathbf{G}^H(\mathbf{x}_k) \mathbf{C}|^2 \sigma_a^2 + \sigma_v^2)$ is the mean of z_k , a nonstationary function of range. The fields must be sampled just slightly above the surface because of the zero boundary condition at the surface. From (10) and (14), note that the RFC problem has been modeled as a nonlinear continuous state space estimation problem. The

objective is now to estimate the parameters of the refractivity \mathbf{g}_k from the PPI observations.

3. Recursive Bayesian Estimation

[20] The classic approach to state estimation in nonlinear state space models is the extended Kalman filter (EKF), which consists of linearizing the state and/or measurement equations using Taylor's series expansions [Gelb, 1974; Anderson and Moore, 1979]. In RFC, an extended Kalman filter approach is problematic because the parameters of interest, i.e., refractivity, appear in the complex exponential in equation (1) which when linearized leads to instability of the EKF and very poor estimates of range-varying refractivity parameters.

[21] For discrete-state sequence estimation problems, the evolution of the state can be described by a lattice where a column of nodes represents the finite number of possible state values at a particular time. Using the Markov property of the state sequence, a computationally efficient method of computing the joint maximum a posteriori (MAP) estimate of the state sequence is the Viterbi algorithm [Forney, 1973], based on dynamic programming. Even though the number of possible sequences grows exponentially with the length of the sequence, the computational complexity of the Viterbi MAP estimate grows only linearly. At least formally, a MAP RFC estimate could be achieved by discretizing the elements of the state \mathbf{x}_k , which contains the refractivity parameters and electromagnetic field, at range, r_k , on fixed grid. Let $\mathbf{x}_{k,j}$ denote the state vector sampled on a

deterministic set of grid points indexed by $j = 1, \dots, J$, at range r_k . The resulting lattice for this discrete state space is shown in Figure 3. Defining $p(\mathbf{x}_1, \dots, \mathbf{x}_K | z_1, \dots, z_K)$ as the joint posterior density of the states up to range K , $f(z_k | \mathbf{x}_k)$ as the likelihood of state \mathbf{x}_k , $k = 1, 2, \dots, K$ and $p(\mathbf{x}_k | \mathbf{x}_{k-1})$ is the transition probability associated with a transition from j th state at range $k-1$ to i th state at range k , the MAP state sequence estimate is defined by

$$\begin{aligned} & \arg \max_{\mathbf{x}_1, \mathbf{x}_2, \dots, \mathbf{x}_K} \{ \log p(\mathbf{x}_1, \dots, \mathbf{x}_K | z_1, \dots, z_K) \} \\ & = \arg \max_{\mathbf{x}_1, \mathbf{x}_2, \dots, \mathbf{x}_K} \left\{ \sum_{k=1}^K \log f(z_k | \mathbf{x}_k) + \log p(\mathbf{x}_k | \mathbf{x}_{k-1}) \right\}. \end{aligned} \quad (15)$$

[22] The Viterbi method finds the optimal path recursively by computing

$$\begin{aligned} W_i(k) = \max_j \{ & W_j(k-1) + \log p_{\mathbf{x}_k | \mathbf{x}_{k-1}}(\mathbf{x}_{k,i} | \mathbf{x}_{k-1,j}) \} \\ & + \log f_{z_k | \mathbf{x}_k}(z_k | \mathbf{x}_{k,i}), \end{aligned} \quad (16)$$

where $W_i(k)$ is the weight of the optimal path terminating at $\mathbf{x}_{k,i}$. The sum in equation (15) corresponds to computing weights $W_i(k)$ for a particular path through the lattice in Figure 3. Note that the total number of state sequences evaluated by equation (16) is J^K which grows exponentially in K . However, the computational complexity of the Viterbi algorithm grows only linearly with K which gives a dramatic reduction in computation. For Markov discrete state sequences, the Viterbi algorithm is guaranteed to find the global MAP estimate.

[23] In the case of a continuous state space, as given in equations (10) and (14), we seek the global maximum to the continuous posterior density $f(\mathbf{X}_k | \mathbf{Z}_k)$, where $\mathbf{X}_k = \mathbf{x}_1, \dots, \mathbf{x}_k$ is a state sequence and $\mathbf{Z}_k = z_1, \dots, z_k$ is the sequence of scalar observations out to range r_k . This maximum could theoretically be estimated using a dense discrete grid of sequence values. To uniformly sample $L + I$ parameters (where L is the number of vertical wave number frequencies propagating and I is the number of refractivity parameters) in \mathbf{x}_k using N values per parameter, requires $J = (L + I)N$ grid points. If the RFC problem were solved using a fixed discretization scheme, we would require an exceptionally large number of grid values, e.g., $N = 3000$, that would render the problem computationally intractable. In this paper therefore we pursue a particle filtering approach [Godsill et al., 2001], the idea is to construct a grid based on realizations $\mathbf{X}_k^{(i)}$ drawn from an appropriate probability distribution, where we denote the i^{th} state sequence realization by $\mathbf{X}_k^{(i)}$. If the support of the density from which these realizations are drawn includes the unknown maximum, then the maximum over the resulting grid has

been shown to asymptotically approach the global maximum in the limit that the number of realizations drawn (and thus the number of grid points) approaches infinity but in practice the solution converges much more quickly [Godsill et al., 2001].

[24] Suppose that the number of realizations (a.k.a. ‘‘particles’’) drawn is J . The number of possible trajectories in the lattice formed by these realizations is then J^K . The posterior density can then be efficiently maximized over these J^K sequences by use of the Viterbi algorithm. An appropriate sampling density must be selected from which to draw the state realizations. In this work, for simplicity, we choose the prior distribution as given by equation (10), augmenting the sequence of each realization \mathbf{X}_{k-1}^i with a new state value \mathbf{x}_k^i , which, because of the Markov property, depends only upon the immediately preceding state value \mathbf{x}_{k-1}^i . An initial prior $p(\mathbf{X}_0)$ given by

$$p(\mathbf{X}_0) = U(\mathbf{g}_0) \delta(\mathbf{v} - \mathbf{v}_0), \quad (17)$$

which is utilized to obtain the initial distribution of the state space, which comprises the refractivity parameters \mathbf{g}_0 and the wave number coefficients \mathbf{v}_0 . A uniform prior on the refractivity parameters $U(\mathbf{g}_0)$ distributed over the parameter space is assumed. The prior on the initial wave number spectrum, \mathbf{v}_0 , corresponds to the radar antenna pattern. From (17), the priors on \mathbf{g}_0 and \mathbf{v}_0 are assumed to be independent.

[25] The state space at any range k is generated from the state space at range $k-1$ by passing the state particles $\mathbf{x}_{k-1,i}$ at range $k-1$ through the state equation (10) to obtain the particles at range k . This transition is indicated by the dotted black lines in Figure 4. This results in a grid, as illustrated in Figure 4, which is the randomly sampled version of continuous state space (as compared to the fixed which is shown in Figure 3). It should be noted that with fine enough sampling in the fixed state space model of Figure 3, the lattice encompasses all possible trajectories whereas in the randomly sampled continuous state space shown in Figure 4, the lattice encompasses all possible trajectories only as the number of samples goes to infinity.

[26] Using the randomly sampled grid, the MAP RFC estimate, by analogy with the discrete state space model, is given by

$$\begin{aligned} & \arg \max_{\mathbf{x}_1^{(i)}, \mathbf{x}_2^{(i)}, \dots, \mathbf{x}_k^{(i)} \forall i} \left\{ \log p(\mathbf{x}_1^{(i)}, \dots, \mathbf{x}_k^{(i)} | z_1, \dots, z_k) \right\} = \\ & \arg \max_{\mathbf{x}_1^{(i)}, \mathbf{x}_2^{(i)}, \dots, \mathbf{x}_k^{(i)} \forall i} \left\{ \sum_{k=1}^K \left[\log f(z_k | \mathbf{x}_k^{(i)}) + \log p(\mathbf{x}_k^{(i)} | \mathbf{x}_{k-1}^{(i)}) \right] \right\}, \end{aligned} \quad (18)$$

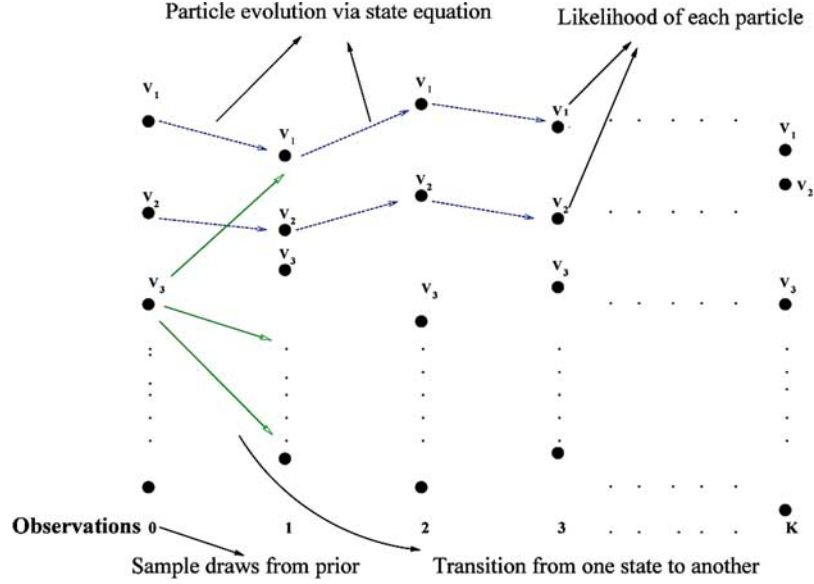


Figure 4. Formulation of particle trajectories as state sequences.

where $\mathbf{x}_1^{(i)}, \mathbf{x}_2^{(i)}, \dots, \mathbf{x}_k^{(i)}$ is the state sequence corresponding to the i th sample in the randomly sampled state space grid of Figure 4. Again, the Viterbi algorithm is used to find the optimal path along all the trajectories by recursively computing

$$W_k^{(i)} = \max_j \left\{ W_{k-1}^{(j)} + \log p_{\mathbf{x}_k | \mathbf{x}_{k-1}}(\mathbf{x}_k^{(i)} | \mathbf{x}_{k-1}^{(j)}) \right\} + \log f_{z_k | \mathbf{x}_k}(z_k | \mathbf{x}_k^{(i)}). \quad (19)$$

[27] As mentioned previously, as the number of samples increases, we cover all possible trajectories in the continuous state space and in the limit that the number of samples goes to infinity, the MAP estimate for the continuous state space problem converges to the true MAP estimator [Godsill *et al.*, 2001]. The advantage of the particle filtering approach is that in practice only a fraction of the number of samples are required when compared to a fixed gridding method.

[28] The algorithm in the MAP RFC method using the Viterbi approach is summarized as follows.

[29] 1. Generation of the randomly sampled distribution of the continuous state space.

a. For $1 \leq i \leq N$, $\mathbf{x}_0^{(i)} \triangleq p(\mathbf{x}_0)$

b. For $1 \leq k \leq K$ and $1 \leq i \leq N$,

$$\mathbf{x}_k^{(i)} = h(\mathbf{x}_{k-1}^{(i)}) + \boldsymbol{\mu}_k^{(i)}$$

[30] 2. Viterbi algorithm for MAP sequence estimation.

a. For $1 \leq i \leq N$,

$$W_0^{(i)} = \log p_{\mathbf{x}_k | \mathbf{x}_{k-1}}(\mathbf{x}_0^{(i)}) + \log f_{z_k | \mathbf{x}_k}(z_k | \mathbf{x}_0^{(i)}),$$

b. For $1 \leq k \leq K$ and for $1 \leq i \leq (L + M)$,

$$W_k^{(i)} = \max_j \{ W_{k-1}^{(j)} + \log p_{\mathbf{x}_k | \mathbf{x}_{k-1}}(\mathbf{x}_k^{(i)} | \mathbf{x}_{k-1}^{(j)}) \} + \log f_{z_k | \mathbf{x}_k}(z_k | \mathbf{x}_k^{(i)})$$

$$\chi_k^{(i)} = \arg \max_{j=1,2,3,\dots,N} \{ W_{k-1}^{(j)} + \log p_{\mathbf{x}_k | \mathbf{x}_{k-1}}(\mathbf{x}_k^{(i)} | \mathbf{x}_{k-1}^{(j)}) \}$$

c. At the last range bin, i.e., $k = K$,

$$\hat{i}_{k_{MAP}} \triangleq \arg \max_{i=1,2,3,\dots,(L+M)} W_k^{(i)}$$

$$\hat{\mathbf{x}}_{k_{MAP}} \triangleq \mathbf{x}_k^{\hat{i}_{k_{MAP}}}$$

d. Trace back to get optimal sequence of refractivity parameters across range.

For $k = K - 1, K - 2, \dots, 2, 1$,

$$i_k = \chi_{k+1}(i_{k+1}),$$

$$\hat{\mathbf{x}}_{k_{MAP}} = \mathbf{x}_k^{(i_k)}$$

[31] Note that the state equation (10) ensures smoothness in field values is maintained by constraining the transition probability density $p(\mathbf{x}_k^{(i)} | \mathbf{x}_{k-1}^{(i)})$. In particular,

for the case where the PE solver step is deterministic, the transition probability density takes on the form, (see Appendix B), given by

$$p(\mathbf{x}_k^{(i)} | \mathbf{x}_{k-1}^{(j)}) = \delta(\mathbf{v}_k^{(i)} - f(\mathbf{v}_{k-1}^{(j)}, \mathbf{g}_k^{(i)})) \Big|_{\mathbf{g}_k^{(i)} = \mathbf{g}_{k-1}^{(j)} + \mathbf{w}_k} \cdot p(\mathbf{g}_k^{(i)} - (\mathbf{g}_{k-1}^{(j)} + \mathbf{w}_k)). \quad (20)$$

[32] If instead of estimating the entire MAP sequence estimate at each range step, we were interested only in the estimating \mathbf{x}_k given data up to range r_k , alternatively the solution for \mathbf{x}_k can be alternatively computed using a filtering approach which maximizes $p(\mathbf{x}_k | z_1, z_2, \dots, z_k)$ at each range r_k . Defining, the forward variable, $\alpha_k^{(i)} \triangleq p(\mathbf{x}_k^{(i)}, z_0, z_1, \dots, z_k)$ where $\alpha_k^{(i)}$ is the joint probability of the data set z_0, z_1, \dots, z_k and the i th sample of state at range r_k , $\mathbf{x}_k^{(i)}$. The forward variable is computed in a recursive manner using the formula [Therrien, 1992]

$$\alpha_k^{(i)} = \left[\sum_{j=1}^I \alpha_{k-1}^{(j)} p(\mathbf{x}_k^{(i)} | \mathbf{x}_{k-1}^{(j)}) \right] p(z_k | \mathbf{x}_k^{(i)}). \quad (21)$$

Once all the forward variable have been computed, the filtered estimates can be easily calculated. In order to do so, calculation of the filtered density function is realized as

$$\alpha_k^{(i)} \triangleq p(\mathbf{x}_k^{(i)}, z_0, z_1, \dots, z_k) \propto p(\mathbf{x}_k^{(i)} | z_0, z_1, \dots, z_k). \quad (22)$$

Thus the filtered distributions are obtained by normalizing the computed forward variables for each of the particle at each range,

$$p(\mathbf{x}_k^{(i)} | D_k) = w_k^{(i)} = \frac{\alpha_k^{(i)}}{\sum_{i=1}^I \alpha_k^{(i)}} \quad (23)$$

The forward MAP estimate based on the marginal distribution of \mathbf{x}_k at each range step r_k is given by

$$\hat{\mathbf{x}}_{k,MAP} = \max_i w_k^{(i)}. \quad (24)$$

In the next section, the Viterbi and forward MAP RFC estimates will be compared in simulations and using real data.

4. Refractivity From Clutter Results

4.1. Simulation Results

[33] In order to evaluate the RFC methods described in the previous section, simulations were performed using 50 realizations of perfectly trilinear profiles were used to

generate 50 range_varying refractivity profiles by means of a simple Markov process as given in equation (2). The simulated range-varying refractivity, along with the initial field which corresponded to the antenna pattern, were then used to predict the field distributions by making use of the split-step Fourier solution to the parabolic equation (PE) given in (1). In the implementation of the split-step PE, the range increments were 200 m and the Fourier transform sizes were of the order of 512. The field was determined up to a height of 200 m with a Hanning window added for heights beyond 200 m so that any reflections from the computational boundary were not significant. The PE solution was used to compute a simulated clutter data using equation (14). This simulated clutter data was then used as ‘‘data’’ to obtain forward MAP and Viterbi MAP sequence estimates of range-varying refractivity.

[34] For the estimation of refractivity, the initial prior on each of the refractivity parameters values was assumed to be uniform and independent of one another. In particular, the base height was assumed to be uniform between 10 and 150 m, thickness was assumed to take on values from 5 to 70 m, M deficit was assumed to be uniform between 0 and 65 M units, while the slope of the mixed layer was assumed to be uniform between -0.13 and 0.13 m/ M units. Five hundred samples of the prior distribution were drawn to represent the set of possible refractivity values at the radar. Similarly, 500 copies of the radar radiation pattern were used to generate the vertical wave number spectrum used in the state vector of equation (9). Thus the 500 samples of the refractivity and the vertical wave number spectrum together represent the set of all possible realizations of the state vector at the radar. Note that this represents a small fraction of the grid points that would be required for fixed uniform sampling. Now, the randomly sampled state space shown in Figure 4 was generated using the method presented in section 3. Once the randomly sampled state space is achieved, we use the particle filtering approach to the Viterbi MAP sequence estimation detailed in section 3 to produce estimates of range-varying refractivity.

[35] We note that in practice, the transition probability governing the wave number spectrum was not considered to be a delta function, but rather a more relaxed condition of a tight uniform distribution was used. This allowed for more diversity in the paths through the lattice which was found to speed convergence. The tight uniform distribution was defined such that transition jumps in the field on the order of 5 dB and less were allowed while jumps greater than 5 dB were not allowed. Thus (20) was actually implemented as

$$p(\mathbf{x}_k^{(i)} | \mathbf{x}_{k-1}^{(j)}) = p\left(E\left(\log\left(\mathbf{v}_k^{(i)} - f\left(\mathbf{v}_{k-1}^{(j)}, \mathbf{g}_k^{(i)}\right)\right)\right)\right) \cdot \Big|_{\mathbf{g}_k^{(i)} = \mathbf{g}_{k-1}^{(j)} + \mathbf{w}_k} \cdot p\left(\mathbf{g}_k^{(i)} - \left(\mathbf{g}_{k-1}^{(j)} + \mathbf{w}_k\right)\right), \quad (25)$$

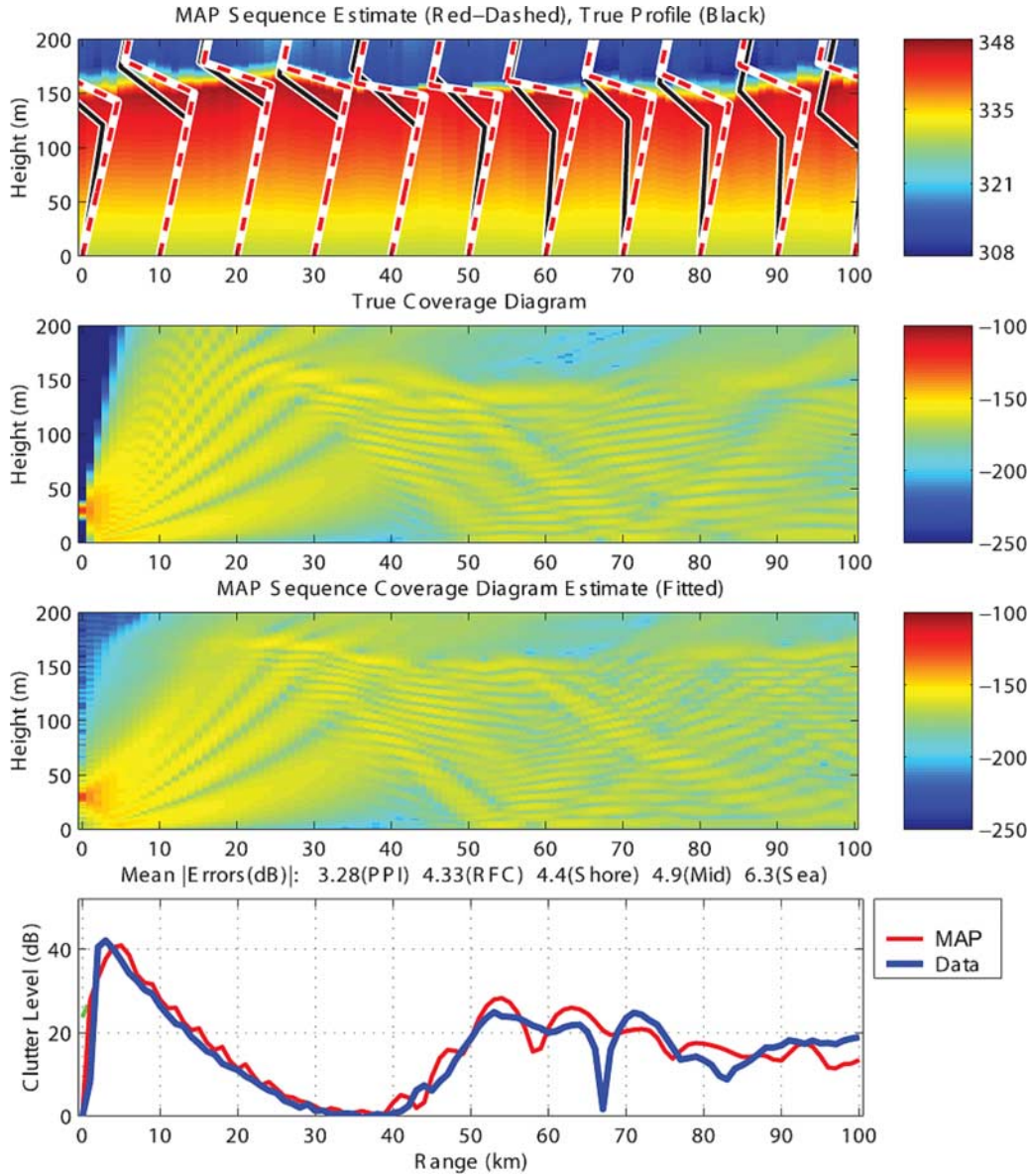


Figure 5. Matched profile result: Viterbi MAP sequence estimation.

where $p(E(\log(Fv_k^{(i)} - f(Fv_{k-1}^{(i)}, g_k^{(i)})))) \sim U[-5, 5]$, E is the expectation operator and F is the inverse Fourier transform operator.

[36] Example RFC results for the scenario described are shown in Figure 5. The top plot of Figure 5 is the comparison of the refractivity estimates with the true refractivity. The absolute average error between the estimated refractivity and the true simulated refractivity was found to be 5.4963 M units. The index of refraction generated using estimates was then passed through the

split-step PE solution to obtain the field distribution over the entire area of coverage. The same procedure was repeated to obtain the field distribution for the true simulated refractivity. As the final goal of the work was the comparison of the true propagation loss to the predicted propagation loss, the propagation loss corresponding to refractivity estimates and the real simulated refractivity were calculated and they are shown as the second and third plots of Figure 5. It can be seen that there is an excellent match between the two propagation

Table 1. Performance Comparison of Forward MAP Estimate and Viterbi MAP Sequence Estimate

Number of Trials	Absolute Average Error in Forward MAP Estimate, dB		Absolute Average Error in Viterbi MAP Sequence Estimate, dB	
	Clutter	Prop Loss	Clutter	Prop Loss
50	4.5234	6.8976	3.6922	6.6087
10	6.0145	6.6473	3.7585	6.6013
12	7.127	7.5123	5.9131	7.0747

loss plots. Now, in order to quantify performance, we define the absolute average error up to a scaling constant as, $\epsilon \triangleq \sum |20 \log_{10}(\frac{\theta_{true}}{\theta_{est}})|$, where θ is the term whose performance is being quantified (e.g., clutter, propagation loss or any of the refractivity parameter values). It should be noted that, when we quantify performance for clutter, the parameter θ is a function of range only whereas, when we quantify performance for propagation loss, the parameter θ is a function of range and height, the average being computed over the entire domain. The error unit is decibels only for the case when we are estimating the error of propagation or clutter loss. Thus the absolute average error, for the entire area of coverage extending from 0 km to 100 km in range and from 0 m to 200 m in height, between the propagation loss corresponding to the refractivity estimates and the propagation loss corresponding to the true refractivity was found to be 4.3304 dB. Finally the field values corresponding to the refractivity estimates were used to generate an estimated clutter data using equations (1) and (14), to enable comparison with the true simulated clutter data generated using the true refractivity profiles as inputs in equations (1) and (14). The bottom plot of Figure 5 contains the solid blue line which is the plot of the data and the estimated clutter data given by the solid red line. It can be seen that the algorithm is able to effectively capture the peaks in the data arising between 50 and 65 km and 70 and 80 km, respectively. The average absolute error between the estimated clutter and the real simulated clutter data was found to be 3.2811 dB.

[37] For over 50 Monte Carlo realizations of range-varying refractivity, the absolute average error between the propagation loss using the true refractivity and the propagation loss using the estimated refractivity are computed and tabulated. The same was done for the absolute average error between the true clutter and the clutter estimate obtained using the estimated refractivity. The results are shown in Table 1. In addition to the Viterbi MAP sequence estimate, the forward algorithm

results were also tabulated for the 50 Monte Carlo realizations. It can be seen that the Viterbi sequence estimate performs better than the forward Monte Carlo estimate because of the ability of the algorithm to update estimates of refractivity at earlier ranges with the arrival of data at later ranges (i.e., step 2d in the algorithm).

4.2. Performance Under Refractivity Model Mismatch Using Real Data

[38] In order to test the robustness of the estimator to mismatches in the perfectly trilinear profile model, simulated clutter data was created using equations (1) and (14) using actual refractivity measurements made by the Applied Physics Laboratory of Johns Hopkins University (APL-JHU) near Wallops Island, Virginia. A helicopter-borne instrument package was flown to and fro (multiple times) from the shore to a distance of approximately 60 km out to sea measuring the refractivity. Each trip of the instrument package is given a case number (10,11,12...22) as illustrated in Figure 6. The solid black lines in Figure 6 are some of the real profile measurements made by the helicopter. Although the ground truth was measured out to 60 km, the data was extended to 100 km by selecting the original measurements again by a simple random walk procedure and this is shown as solid dark lines in Figure 7. The same assumptions of uniform prior generated in the case of perfectly matched profiles simulations were used for this scenario also. Estimates of range-varying refractivity were then obtained using the Viterbi MAP sequence estimate from the simulated clutter data. Using these estimates of refractivity, the propagation loss over the area of coverage was generated using equation (1). A typical result for the scenario described is shown in Figure 7. In the top plots of Figure 7, the range-varying refractivity estimates (dashed lines) are compared to the true range-varying refractivity values (solid lines). Note that the refractivity estimates match closely to the measurements and even capture the range variations of the refractivity quite accurately. The absolute mean value of the error between the ground truth refractivity measurements and the estimated range-varying refractivity, taken over the entire area of coverage, namely, over range from 0 km to 100 km and height from 0 m to 200 m, was 3.8673 M units. Similar to Figure 5 of the matched profile scenario, the comparison of clutter obtained using estimates of refractivity in equations (1) and (14) and that of the of actual clutter, as well as the simulated propagation loss and the true propagation loss plots are indicated by the bottom three plots. The absolute average error between the propagation loss computed using the estimates of refractivity and those computed using the ground truth was found to be 6.2493 dB. Finally, the estimated clutter was generated in the same manner

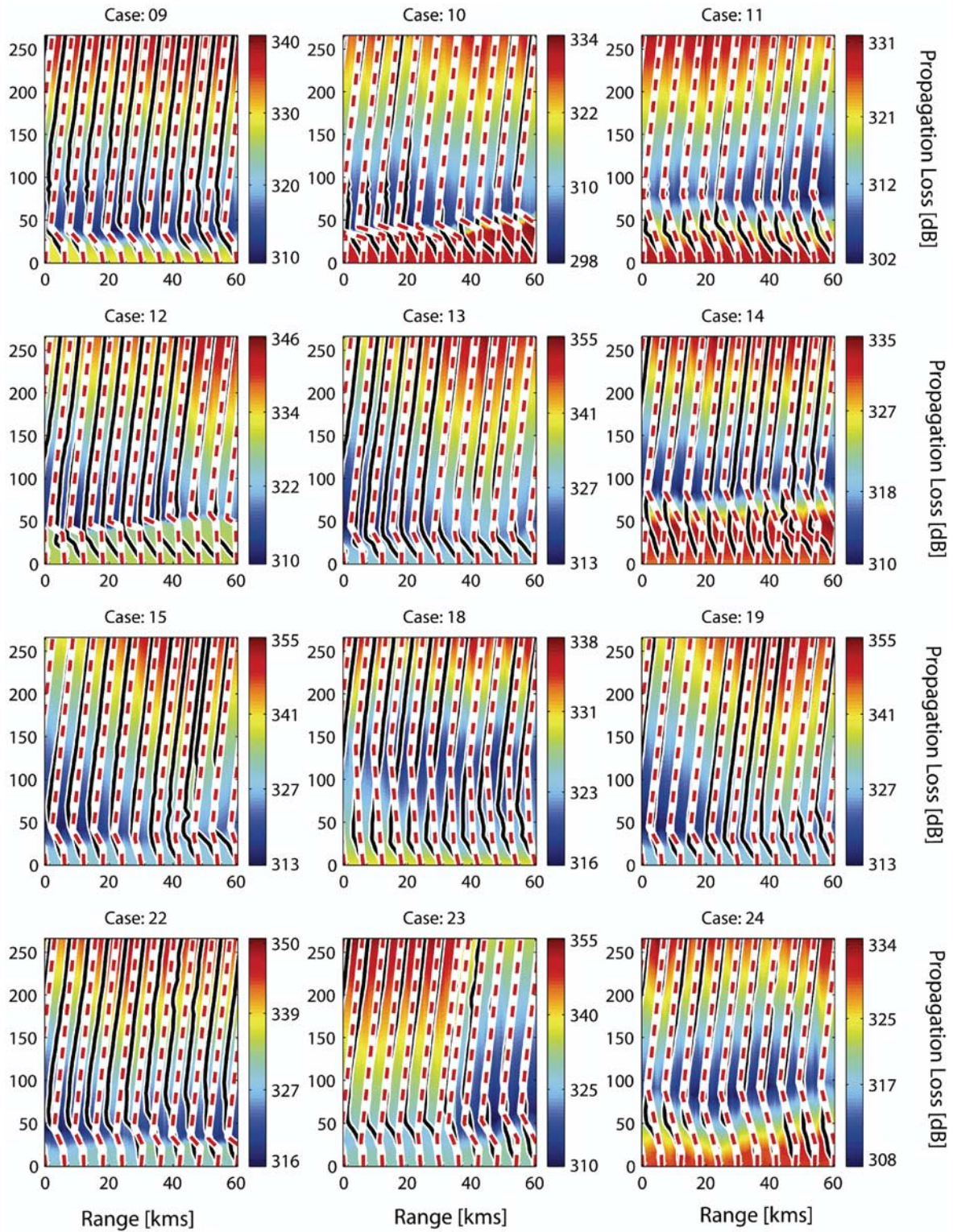


Figure 6. Real data profile fits. Dashed line profiles show RFC Viterbi MAP sequence estimates. Solid line profiles show true helicopter profiles.

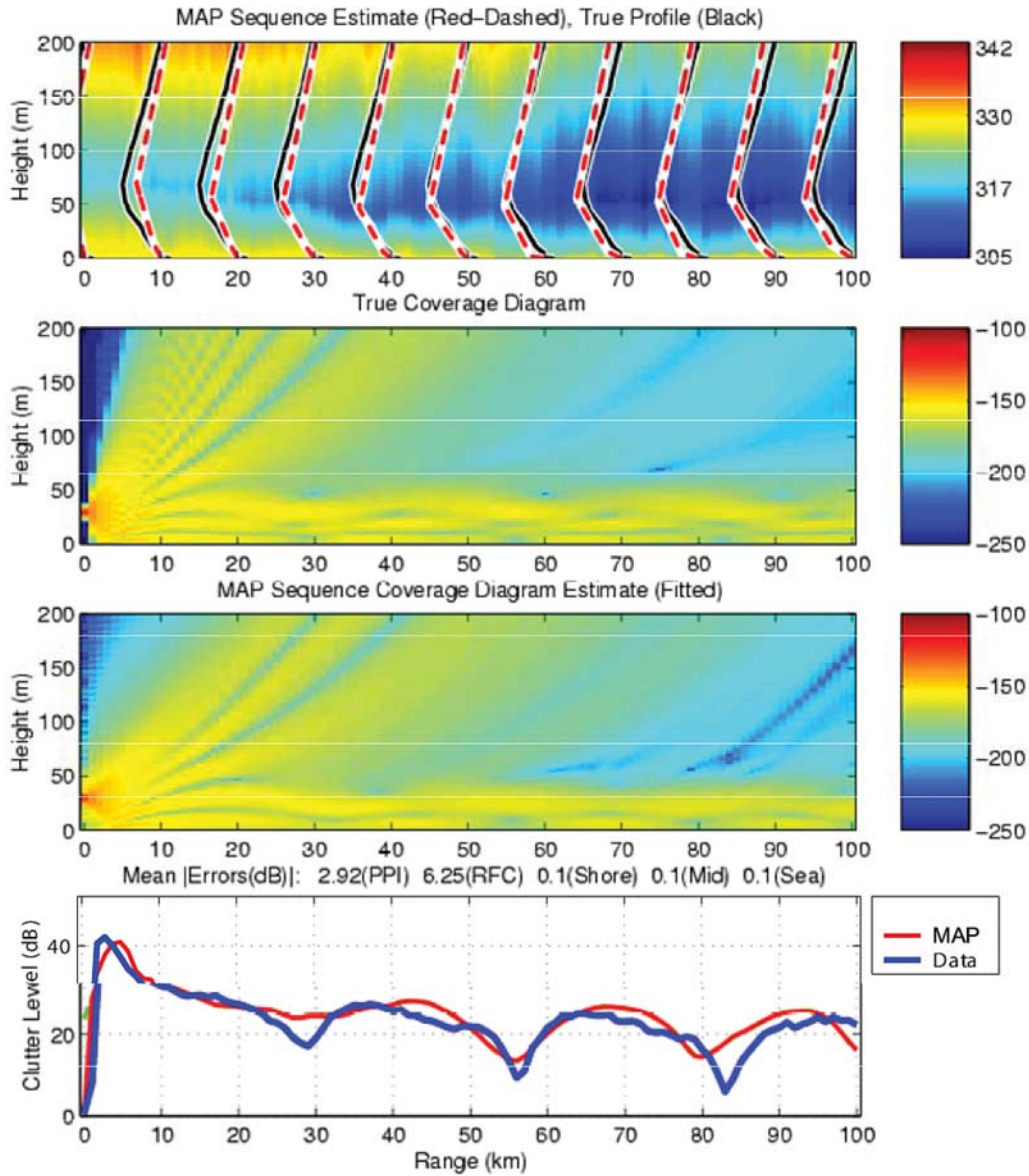


Figure 7. Mismatched profile result: Viterbi MAP sequence estimation.

as in the matched profile case and it was compared to the true simulated clutter as shown in the fourth plot of Figure 7. The absolute average error between the estimated clutter and the true clutter for the plot shown is 2.9162 dB. For 10 Monte Carlo realizations mismatched refractivity, the average absolute error in propagation loss is tabulated in Table 1. As illustrated in Table 1, even under mismatch, the Viterbi MAP sequence estimate method performs much better than the results obtained using the forward algorithm estimates.

4.3. Real Data Results

[39] To test RFC with real clutter, data was collected on 2 April 1998 using the Space and Range radar (SPANDAR) located at Wallops Island, Virginia. The radar transmitter/receiver is approximately 30 m high and was operating at a frequency of 2.85 GHz with a pulse width of 1μ sec and a pulse repetition frequency of 500 Hz. Real clutter data was measured at azimuths ranging from 0° to 360° at intervals of 0.4° . At each azimuth, data was collected from 0 km to approximately

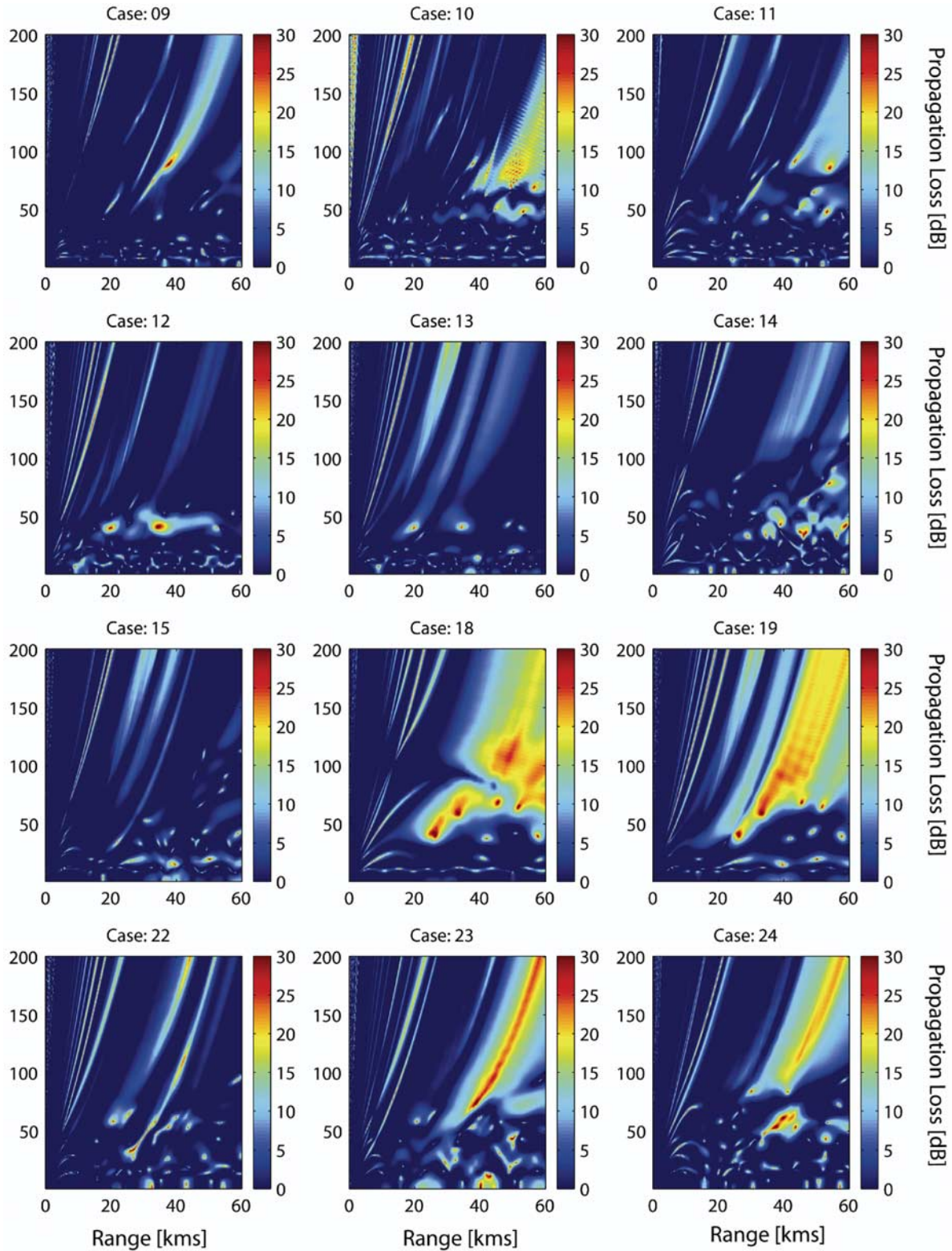


Figure 8. Errors in propagation loss for real data cases for Viterbi MAP sequence estimates.

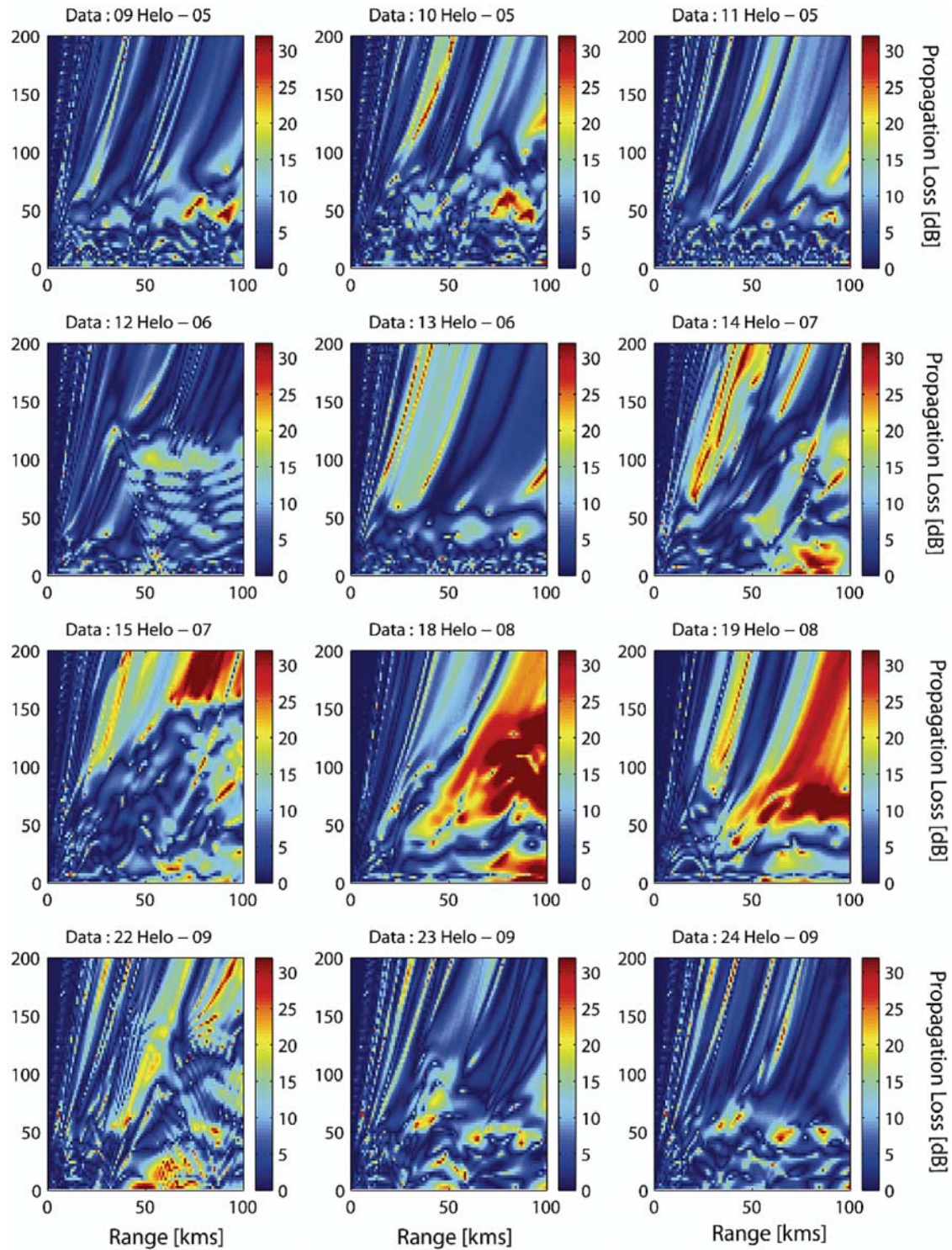


Figure 9. Errors in propagation loss for real data case for forward MAP estimates.

260 km at increments of 600 m. Figure 6 shows the comparison between the range-varying refractivity obtained using the real clutter data and the ground truth refractivity measurements made using a helicopter as described earlier. It can be seen from these plots that the features of the duct, especially its range-varying nature are captured in most cases. Figure 8 illustrates the average absolute error between the propagation loss estimates obtained using the Viterbi MAP sequence estimates of refractivity and the propagation loss generated by using the ground truth refractivity data. For completeness, in Figure 9 we also included the results for the forward MAP method which performed less well. This is due to the ability of the MAP sequence estimate to update estimates at earlier ranges with the arrival of new data thus reducing the propagation of any error in estimates down the range. It can also be seen from Figure 8 that the error is minimal within the duct. The majority of the error contributions arise in areas outside the duct. The average absolute error in quantities propagation loss and clutter were calculated for the 12 real data cases and tabulated in Table 1. Once again, it can be seen that the Viterbi MAP sequence estimate gives better performance than the forward MAP filtered estimates.

5. Conclusion

[40] This paper has shown how recursive Bayesian estimation when combined with forward and Viterbi algorithms can be used to solve the problem of estimating RFC in a sequential manner. This scheme provides a way of quickly obtaining propagation loss estimates under complicated ducting conditions. The simulation and the real data results clearly show that the propagation loss estimates obtained from RFC are comparable to those obtained from ground truth refractivity measurements. Comparison of the Viterbi and forward algorithm results indicate that it is critical to update the estimate of refractivity at all ranges with the arrival of new data in order to obtain good performance. In the work presented, we have represented a continuous state space by sparse number of samples obtained by sampling from a simplistic prior distribution. Further work is necessary to determine more sophisticated methods of sampling the continuous state space in order to obtain very accurate results and faster convergence of the algorithm by sampling from distributions that are data adaptive.

Appendix A

[41] Let us define $r_n(k) \triangleq \frac{|y_n(k)|}{\sigma_\phi^2/2}$, where

$$\begin{aligned} \sigma_\phi^2 &\triangleq \text{Var}(y_n(k)) \\ &= |L(x_k; \mathbf{g})|^2 \sigma_a^2 + \sigma_v^2. \end{aligned} \quad (\text{A1})$$

Then the clutter data can be written as

$$z_k = \frac{10}{N \log 10} \sum_{n=1}^N \log(r_n(k)) + \frac{10}{\log 10} \log\left(\frac{\sigma_\phi^2}{2}\right). \quad (\text{A2})$$

The mean of the random variable statistical model of the clutter data z_k is given by

$$\begin{aligned} E(z_k) &= \frac{10}{N \log 10} \sum_{n=1}^N E(\log(r_n(k))) \\ &\quad + \frac{10}{\log 10} \log\left(\frac{\sigma_\phi^2}{2}\right). \end{aligned} \quad (\text{A3})$$

[42] Since the clutter returns are independent and identically distributed (i.i.d.), the expectation does not depend on the snapshots. Hence the above equation becomes

$$E(z_k) = \frac{10}{\log 10} E(\log(r_n(k))) + \frac{10}{\log 10} \log\left(\frac{\sigma_\phi^2}{2}\right). \quad (\text{A4})$$

The random variable (r.v.) $r_n(k)$ is chi-square distributed with 2 degrees of freedom, as it is the modulus squared of a complex r.v. The term $E(\log(r_n(k)))$ can be shown to be equal to $(\log(2) - \gamma)$, where γ is Euler's number. Thus the equation reduces to the form

$$E(z_k) = \frac{10}{\log 10} E(\log(2) - \gamma) + \frac{10}{\log 10} \log\left(\frac{\sigma_\phi^2}{2}\right). \quad (\text{A5})$$

Substituting (A1) in (A5) and by simple algebraic manipulation, we get

$$E(z_k) = \frac{10}{\log(10)} \log\left(|L(x_k; \mathbf{g})|^2 \sigma_a^2 + \sigma_v^2\right) - \frac{10\gamma}{\log(10)}. \quad (\text{A6})$$

Similarly, the variance of the clutter data can be proven to be

$$\begin{aligned} \text{Var}(z_k) &= \left(\frac{10}{N \log(10)}\right)^2 \text{Var}(\log(r_n(k))) \\ &= \left(\frac{10}{N \log(10)}\right)^2 \left[\frac{\pi^2}{6} + (\log(2) - \gamma)^2\right]. \end{aligned} \quad (\text{A7})$$

Appendix B

[43] The transition probability can be written as

$$p(\mathbf{x}_{k,i}|\mathbf{x}_{k-1,j}) = \int p(\mathbf{x}_{k,i}|\mathbf{x}_{k-1,j}, \boldsymbol{\mu}_k) p(\boldsymbol{\mu}_k) d\boldsymbol{\mu}_k, \quad (\text{B1})$$

where $\boldsymbol{\mu}_k$ is the state noise given in (10).

[44] Now, splitting the terms of the state vector into the field components and the refractivity parameter components, we get

$$p(\mathbf{x}_{k,i}|\mathbf{x}_{k-1,j}) = \int \int p(\mathbf{u}_{k,i}, \mathbf{g}_{k,i}|\mathbf{u}_{k-1,j}, \mathbf{g}_{k-1,j}, \mathbf{w}_g, \mathbf{w}_u) \times p(\mathbf{w}_g, \mathbf{w}_u) d\mathbf{w}_g d\mathbf{w}_u, \quad (\text{B2})$$

where \mathbf{w}_g and \mathbf{w}_u are the noise associated with the refractivity parameters and the field in the state equation.

[45] Assuming that the joint probability of the noise can be separated as the product of the marginal probabilities, corresponding to noise in refractivity parameters and that in the field, we get, separating the integrals,

$$p(\mathbf{x}_{k,i}|\mathbf{x}_{k-1,j}) = \int \int p(\mathbf{u}_{k,i}|\mathbf{g}_{k,i}, \mathbf{u}_{k-1,j}, \mathbf{g}_{k-1,j}, \mathbf{w}_g, \mathbf{w}_u) \times p(\mathbf{g}_{k,i}|\mathbf{u}_{k-1,j}, \mathbf{g}_{k-1,j}, \mathbf{w}_g, \mathbf{w}_u) p(\mathbf{w}_g) d\mathbf{w}_g p(\mathbf{w}_u) d\mathbf{w}_u. \quad (\text{B3})$$

However, the conditional distribution on the refractivity parameter, \mathbf{u}_k , is simply a delta function since given all the other terms, it is purely deterministic. Hence the integral is simplified into

$$\begin{aligned} p(\mathbf{x}_{k,i}|\mathbf{x}_{k-1,j}) &= p(\mathbf{u}_{k,i}|\mathbf{g}_{k,i}, \mathbf{u}_{k-1,j}, \mathbf{g}_{k-1,j}, \mathbf{w}_g, \mathbf{w}_u) p(\mathbf{w}_g)|_{\mathbf{g}_{k,i}=\mathbf{g}_{k-1,j}+\mathbf{w}_k} \\ &= \delta(\mathbf{u}_{k,i} - f(\mathbf{u}_{k-1,j}, \mathbf{g}_{k,i}))|_{\mathbf{g}_{k,i}=\mathbf{g}_{k-1,j}+\mathbf{w}_k} \\ &\quad \cdot p(\mathbf{g}_{k,i} - (\mathbf{g}_{k-1,j} + \mathbf{w}_k)). \end{aligned} \quad (\text{B4})$$

[46] **Acknowledgments.** The authors would like to acknowledge the work by Joseph Tabrikian, currently with Ben-Gurion University, Ber-Sheva, Israel, in the derivation of the clutter model and also in the development of some of the preliminary ideas associated with the Markov model for field propagation in the troposphere.

References

- Anderson, B. D., and J. B. Moore (1979), *Optimal Filtering*, Prentice-Hall, Upper Saddle River, N. J.
- Anderson, K. D. (1994), Tropospheric refractivity profiles inferred from low elevation angle measurements of global positioning system signal, *AGARD Conf. Proc.*, 567, 2-1–2-7.
- Barrios, A. (2004), Estimation of surface-based duct parameters from surface clutter using a ray trace approach, *Radio Sci.*, 39, RS6013, doi:10.1029/2003RS002930.
- Dockery, G. D. (1998), Modeling electromagnetic wave propagation in the troposphere using the parabolic equation, *IEEE Trans. Antennas Propag.*, 36, 1464–1470.
- Dockery, G. D., and J. R. Kuttler (1996), An improved impedance-boundary algorithm for Fourier split-step solutions of the parabolic wave equation, *IEEE Trans. Antennas Propag.*, 44, 1592–1599.
- Forney, G. D. (1973), The Viterbi algorithm, *Proc. IEEE*, 61(3), 268–278.
- Gelb, A. (1974), *Applied Optimal Estimation*, MIT Press, Cambridge, Mass.
- Gerstoft, P., L. T. Rogers, W. S. Hodgkiss, and L. J. Wagner (2003a), Refractivity estimation using multiple elevation angles, *IEEE J. Oceanic Eng.*, 28, 513–525.
- Gerstoft, P., L. T. Rogers, J. L. Krolik, and W. S. Hodgkiss (2003b), Inversion for refractivity parameters from radar sea clutter, *Radio Sci.*, 38(3), 8053, doi:10.1029/2002RS002640.
- Godsill, S., A. Doucet, and M. West (2001), Maximum a posteriori sequence estimation using Monte Carlo particle filters, *Ann. Inst. Stat. Math.*, 53(1), 82–96.
- Gossard, E. E., and R. G. Strauch (1983), *Radar Observation of Clear Air and Clouds*, Elsevier, New York.
- Halvey, R. A. (1983), Radiosonde errors and spurious surface-based ducts, *Proc. IEEE, Part F*, 130, 643–648.
- Richter, J. H. (1969), High resolution tropospheric radar sounding, *Radio Sci.*, 4(12), 1261–1268.
- Rogers, L. T. (1996), Effects of the variability of atmospheric refractivity on propagation estimates, *IEEE Trans. Antennas Propag.*, 44, 60–465.
- Rowland, J. R., and S. M. Babin (1987), Fine-scale measurements of microwave refractivity profiles with the helicopter and low-cost rocket probes, *Johns Hopkins APL Tech. Dig.*, 8(4), 413–417.
- Skolnik, M. I. (1980), *Introduction to Radar Systems*, McGraw-Hill, New York.
- Tabrikian, J., and J. L. Krolik (1999), Theoretical performance limits on tropospheric refractivity estimation using point-to-point microwave measurement, *IEEE Trans. Antennas Propag.*, 47, 1727–1734.
- Tabrikian, J., J. L. Krolik, and S. Vasudevan (1999), Estimating tropospheric refractivity parameters from radar sea clutter, in *Proceedings of the IEEE Signal Processing Workshop on Higher-Order Statistics*, pp. 345–348, IEEE Press, Piscataway, N. J.
- Therrien, C. W. (1992), *Discrete Random Signals and Statistical Signal Processing*, Prentice-Hall, Upper Saddle River, N. J.
- Vasudevan, S., and J. L. Krolik (2001), Refractivity estimation from radar clutter by sequential importance sampling with a Markov model for microwave propagation, paper presented at International Conference on Signals, Systems and Com-

munications (ICASSP 2001), Inst. of Electr. and Electron. Eng. Signal Process. Soc., Salt Lake City, Utah.

R. Anderson, Applied Signal Technology, Inc., 1555 Wilson Blvd, Suite 703, Arlington, VA 22209, USA. (richard_anderson@appsig.com)

P. Gerstoft, Marine Physical Laboratory, Scripps Institution of Oceanography, UCSD, La Jolla, CA 92093, USA. (gerstoft@mpl.ucsd.edu)

S. Kraut, Lincoln Laboratory, MIT, 244 Wood Street, Lexington, MA 02420, USA. (kraut@ll.mit.edu)

J. L. Krolik, Department of Electrical and Computer Engineering, Duke University, Durham, NC 27708-0291, USA. (jk@ee.duke.edu)

L. T. Rogers, Space and Naval Warfare Systems Center, Code D858, San Diego, CA 92152, USA. (trogers@spawar.navy.mil)

S. Vasudevan, Sensor Research and Development Corporation, Orono, ME 04473, USA. (svasudevan@srdcorp.com)